International Journal of Nanomedicine

Dovepress
Taylor & Francis Group

Open Access Full Text Article

ORIGINAL RESEARCH

Ti_3C_2Tx MXene Potentiates PSAT1-Mediated Osteogenesis Through miR-665/GSK-3β/β-Catenin Axis to Counteract Inflammation-Induced Bone Loss

Jinlong Zhang[1,2,*], Xinyang Wang[3,4,*], Jingwen Xiao[5,*], Hongxiang Hong[1,2], Jiajia Chen[1,2], Chunshuai Wu[1,2], Guanhua Xu[1,2], Zhiming Cui[1,2]

[1]Department of Spine Surgery, Nantong City No.1 People's Hospital and Second Affiliated Hospital of Nantong University, Nantong, Jiangsu Province, 226001, People's Republic of China; [2]Research Institute for Spine and Spinal Cord Disease of Nantong University, Nantong, Jiangsu, 226014, People's Republic of China; [3]Department of Stomatology, Affiliated Hospital of Nantong University, Medical School of Nantong University, Nantong, Jiangsu Province, 226001, People's Republic of China; [4]Department of Stomatology, Zhenjiang 359 Hospital, Zhenjiang, Jiangsu Province, 212000, People's Republic of China; [5]Department of Stomatology, Haimen District People's Hospital, Nantong, Jiangsu Province, 226100, People's Republic of China

*These authors contributed equally to this work

Correspondence: Zhiming Cui; Guanhua Xu, Department of Spine Surgery, Nantong City No.1 People's Hospital and Second Affiliated Hospital of Nantong, Nantong, Jiangsu Province, 226001, People's Republic of China, Email czmspine@ntu.edu.cn; xghspine@163.com

Introduction: Inflammatory signaling-induced stem cell dysfunction severely impairs bone regeneration. This study aimed to develop a combinatorial strategy using $Ti_3C_2T_x$ MXene scaffolds and PSAT1-engineered dental pulp stem cells (oe-PSAT1 DPSCs) to counteract inflammation-mediated osteogenic suppression.

Methods: Dental pulp stem cells (DPSCs) were treated with TNF-α to simulate an inflammatory microenvironment. miR-665 expression and its targeting relationship with PSAT1 were analyzed via qRT-PCR, dual-luciferase reporter assay, and Western blot. The role of the miR-665/PSAT1/GSK-3β/β-catenin axis in osteogenic differentiation was evaluated using ALP activity, alizarin red staining, and immunofluorescence. $Ti_3C_2T_x$ MXene was synthesized and characterized, and its effects on ROS scavenging and osteogenesis were assessed in vitro. In vivo efficacy was validated using a rat calvarial defect model with micro-CT, histological staining, and immunohistochemistry.

Results: TNF-α stimulation upregulated miR-665, which directly targeted PSAT1 and inhibited the GSK-3β/β-catenin pathway, suppressing DPSCs osteogenic differentiation. PSAT1 overexpression rescued this suppression. $Ti_3C_2T_x$ MXene scavenged ROS, enhanced calcium-dependent mineralization, and synergized with oe-PSAT1 DPSCs to amplify β-catenin activation. In rat models, the $Ti_3C_2T_x$ MXene /oe-PSAT1 DPSCs combination achieved superior bone defect closure (higher BV/TV, Tb. Th, and mature collagen deposition) compared to $Ti_3C_2T_x$ MXene alone.

Discussion: This study identifies the miR-665/PSAT1/GSK-3β/β-catenin axis as a key regulator of inflammatory osteogenesis. The $Ti_3C_2T_x$ MXene/oe-PSAT1 DPSCs strategy concurrently neutralizes oxidative stress and activates osteogenic signaling, providing a translatable platform for inflammatory bone regeneration.

Keywords: DPSCs, osteogenic differentiation, miR-665, PSAT1, Ti_3C_2Tx

Introduction

Recent advances in bone tissue engineering have highlighted the synergistic potential of stem cells and bioactive scaffolds to address critical-sized bone defects.[1,2] Among various stem cell sources, dental pulp stem cells (DPSCs) have emerged as particularly promising candidates due to their accessibility, multilineage differentiation capacity, and low immunogenicity.[3] On the other hand, DPSCs with multiple differentiation potential, self-renewal, and injury repair are suitable in bone tissue engineering.[4] Therefore, the complex and specific molecular mechanisms which involve in osteogenic differentiation of DPSCs are necessary to further study to extend their clinical application.

Received: 9 March 2025
Accepted: 15 August 2025
Published: 12 September 2025

Graphical Abstract

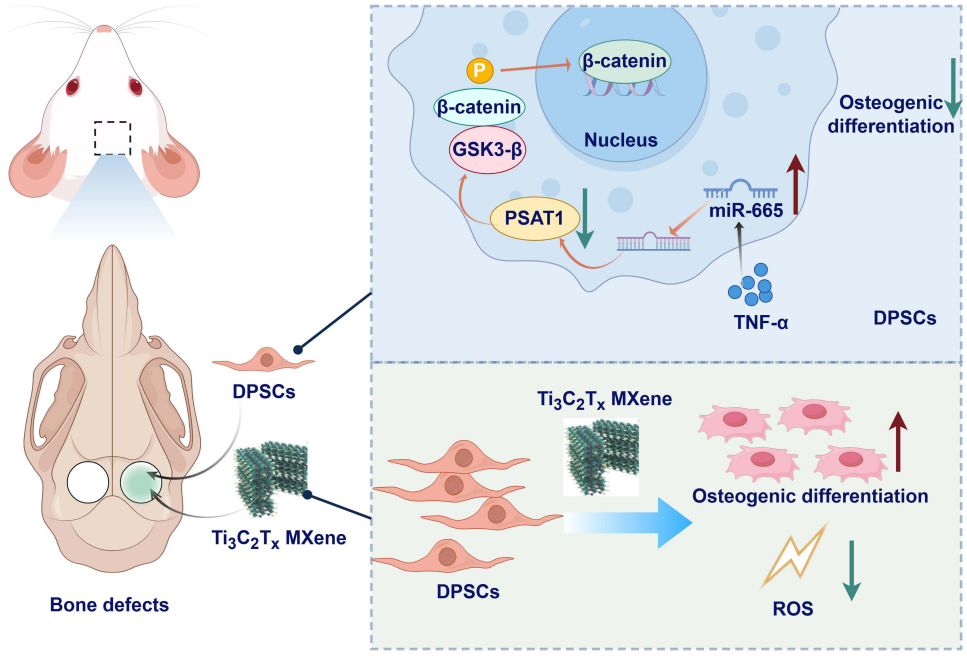

Surgical injury, trauma, and some other diseases, such as periodontitis, trigger innate immunity.[5] An optimal level of immune activation often showed a positive effect on tissue repair and regeneration.[5] Many inflammatory factors, lipopolysaccharide (LPS), TNF-α as well as interleukin family, Engaged in the immune response during the healing of bone tissue defects.[5,6] In dental implantation, the surface material of implants influenced the inflammatory driving process in surrounding areas,[7] which meant scaffold materials played key roles in microenvironment regulation during bone tissue repair. Previous studies also proved that mild inflammatory stimulation promoted osteogenic differentiation of DPSCs, while highly inflammatory stimulation had negative results.[8] As is known to all, TNF-α is an inflammatory factor showing in a variety of inflammatory diseases,[8] and the concentration of TNF-α is correlated with periodontitis activity.[9] How to eliminate the negative effects of inflammation on osteogenesis is the focus of clinical research.

MicroRNAs (miRNAs or miRs), which have 18–25 nucleotides-long non-coding RNAs, are responsible for target genes after transcription by directly binding to the 3'-untranslated regions (UTRs) of the mRNA.[10] There is strong evidence that miRNAs are involved in inflammatory regulation as well as osteogenic differentiation of stem cells.[11] Upregulating the miR-665's expression level promoted the progress of inflammatory bowel diseases.[12] In septic acute kidney injury (AKI), the miR-665's expression level was upregulated, while the inflammation and apoptosis of HK-2 cells caused by LPS were significantly suppressed when inhibition of miR-665 was repressed, resulting in the decrease in kidney injury.[13] In terms of odontoblast differentiation of stem cells, miR-665 was proved to act as a repressor of odontoblast differentiation and mineralization by targeting K (lysine) acetyltransferase 6a (KAT6A).[14] Also, miR-665 was found regulating as a repressor in osteogenic differentiation of adipose-derived stem cells (ADSCs), which could be sponged by extended non-coding RNA HIF1A-AS2 and then activated the PI3K/AKT signaling pathway to promote osteogenic differentiation.[15] However, their study focused on ASCs and did not explore the role of miR-665 in inflammatory microenvironments. Thereby, it is important to investigate how miR-665 affects DPSCs's osteogenic differentiation.

PSAT1 acts as the key enzyme in serine metabolism and cooperates with phosphoglycerate dehydrogenase (PHGDH), phosphoserine phosphatase (PSPH), and serine hydroxymethyltransferase (SHMT) to transform 3-phosphoglycerate (3-PG) into L-serine.[16] PSAT1 dysregulation often results in aberrant serine metabolism, and it has been proven as an oncogene in lung, colorectal, ovarian cancer and osteosarcoma.[17–20] On the other hand, serine metabolism takes part in

the survival and differentiation capacity of stem cells, and the decrease of serine metabolism in DPSCs often causes aging and stemness capacity loss.[21] As the critical enzyme in serine metabolism, PSAT1 knockdown mouse embryonic stem cells (ESCs) lost their potentials of differentiation.[22] In addition, increased expression of PSAT1 in the treatment inflammation medium (TNF-α and ascorbic acid/retinol) accompanied by multilineage differentiation potential of gingival-MSCs.[23] However, these studies did not clarify whether PSAT1 participates in osteogenic differentiation of DPSCs or its regulatory relationship with miRNAs like miR-665.

Recent research has shown Ti_3C_2 MXene represents a noteworthy example of 2D nanomaterials that promises significant potential owing to its biocompatibility, high near-infrared (NIR) absorption, and efficient photothermal conversion capabilities.[24,25] Although some studies have indicated the potential of Ti_3C_2 MXene to enhance osteogenesis in mesenchymal stem cells, the impact on DPSCs osteogenic differentiation inadequately explored.[26] However, prior research primarily focused on MXene's single mechanism or its effect on other stem cells, with limited exploration of its interplay with genetic engineering or its role in scavenging ROS to mitigate inflammatory damage. This study elucidates the miR-665/PSAT1/GSK-3β/β-catenin signaling pathway as a critical regulator of DPSCs osteogenic differentiation under inflammatory conditions. Additionally, Ti_3C_2Tx MXene demonstrates promising potential in bone tissue engineering by enhancing osteogenic differentiation and promoting bone regeneration. These findings provide a novel therapeutic strategy for inflammation-related bone defects.

Materials and Methods

Cell Cultures

Healthy and normal third molars were extracted from the patients (age at 18 ~ 28 years, n=7) who underwent treatment in the Stomatological Department with the informed consent approved by the Ethics Committee of Haimen district people's hospital (Approval Number: 2024-KY44-01). This study involving human third molars was conducted in accordance with the principles of the Declaration of Helsinki. All specimens without carious lesions or any other oral infection were used in this study. After extracting pulp tissue from third molars, the tissue was minced into 1 mm^3 fragments and digested in a solution containing 3 mg/mL type I collagenase, 4 mg/mL dispase, and 1% penicillin/streptomycin in phosphate-buffered saline (PBS, Sangon Biotech, E607008-0500) at 37°C for 1 h with gentle shaking. The digested suspension was filtered through a 70 μm strainer (BD Falcon) to obtain single cells, which were then seeded in DMEM/F12 (HyClone, SH30023.01B) supplemented with 10% fetal bovine serum (FBS, Sigma, 12003C) and 1% penicillin/streptomycin. Cultures were maintained at 37°C in 5% CO_2, with medium changed every 3 days. Cell passage was performed using 0.25% trypsin-EDTA when confluence reached 85–90%, and passage 3 (P3) cells were used for experiments to ensure consistency. We adopted part of the experimental methods described in the referenced study[27] Our previous study has characterized specific cellular markers of DPSCs by flow cytometry as the results of positive expression in CD29 and CD105, while negative expression in CD31 and CD34.[28]

Osteogenic Differentiation

6-well plates were used to cultured DPSCs, and cells were seeded at 5×10^4 / well. Cells were cultured in the osteogenic induction medium (OIM) (DMEM containing 10% FBS, 0.1 μM dexamethasone (Sigma, D4902), 10 mM β-glycerophosphate (Sigma, G9422), and 50 μg/mL vitamin C (Sigma, A4403). DPSCs were differentiated with or without TNF-α (10, 20 ng/mL, Sigma, T6674) for 7, 14 and 21 days. Every three days, the medium was changed and TNF-α was added.

Mineralization Formation and ALP Activity

After incubated in OIM, DPSCs were fixed with 4% paraformaldehyde (PFA, Sangon Biotech, E672002-0500) at room temperature for 1 hour and washed by PBS 3 times. Cells were stained with alizarin red S for 10 mins (Beyotime, Shanghai, China, C0148S). The absorbance at 570 nm was measured. The Alkaline phosphatase (ALP) activity was performed by the ALP assay kit according to the manufacturer's protocols (Beyotime, Shanghai, China, P0321S).

Western Blot

This method showed the relative expression of osteogenic differentiation marker proteins, miRNA's target proteins, and signaling pathway proteins. Cells were lysed in a buffer consisting of 50 mM TRIS, 150 mM NaCl, 2% sodium dodecyl sulfate (SDS), and a protease inhibitor mixture. Bradford assay (Bio-Rad) was used to determine protein concentrations after centrifugation at 12,000 rpm for 15 mins. The resulting supernatant (50 μg of protein) was separated by SDS-polyacrylamide gel electrophoresis (PAGE) and transferred onto 0.45 mm PVDF membranes at 300 mA for 150 mins in a blotting apparatus (Bio-RAD, CA, USA). Membranes were blocked with 5% non-fat milk for 2 hours and incubated with primary antibodies (1:1000) at 4 °C overnight. Subsequently, after washing three times with TBST, PVDF membranes were washed with TBST and incubated with HRP-conjugated secondary antibodies (1:10000) at room temperature for 2 hours. GAPDH was served as the internal reference.

The primary antibodies were showed as following: GAPDH (anti-rabbit, Proteintech), PSAT1 (anti-rabbit, Proteintech, 10494-1-AP), BMP2 (anti-mouse, Proteintech, 66383-1-Ig), RUNX2 (anti-rabbit, Cell Signaling Technology, 12556), OPN (anti-rabbit, Proteintech, 22952-1-AP), β-catenin (anti-rabbit, Proteintech, 51067-2-AP), p-β-catenin (anti-rabbit, Proteintech, 80067-1-RR), GSK-3β (anti-rabbit, Proteintech, 22104-1-AP), p-GSK-3β (anti-rabbit, Proteintech, 14850-1-AP).

Immunofluorescent Staining

DPSCs were washed with PBS and then fixed with 4% PFA for 1 hour. Then DPSCs were washed by PBS with 0.1% Triton X-100 (PBST) and blocked in PBST containing 10% FBS for 30 min. Then, cells were incubated with primary antibodies against PSAT1 (1:50; anti-rabbit, Proteintech, 10494-1-A), RUNX2 (1:50; anti-rabbit, Cell Signaling Technology, 12556), OPN (1:50; anti-rabbit, Proteintech, 22952-1-AP), β-catenin (1:50; anti-rabbit, Abcam, ab224803) at 4 °C for 24 hours, or Phalloidin-Fluorescein conjugate for 2 h, and subsequently washed by TBST and incubated in secondary antibody for 2 hours at room temperature. Nuclei stained with 4' 6-diamidino-2-phenylindole (DAPI) (1:800, Abcam, ab228549). Representative images were observed by a Leica fluorescence microscope (Germany).

Quantitative Real-Time PCR

TRIzol (TaKaRa, Bio) was used to extract total RNA from DPSCs. Complementary DNA (cDNA) for miRNA was synthesized by the Transcript® miRNA First-Strand cDNA Synthesis SuperMix Kit (Full Golden Bio, China). Real-time PCR was applied to measure the expression of the miRNAs through a miDETECT A Track™ miRNA quantitative real-time PCR (qRT-PCR) Starter Kit (RIBOBIO, Guangzhou, China). U6 was tested as a reference factor. Relative gene expression level was performed by the $2^{-\Delta\Delta Ct}$ method. The primer sequences: miR-665, F: 5'-GGTCTACAAAGGGAAGC-3', R: 5'-TTTGGCACTAGCACATT-3', U6, F: 5'-CGCTTCGGCAGCACATATACTAA-3', R: 3'-TATGGAACGCTTCACGAATTTGC −5'.

Dual-Luciferase Reporter Gene Assay

The wild-type (WT) and mutant type (MUT) 3'-untranslated regions (3'UTRs) of PSAT1, which contain or not the binding site for miR-665, respectively, were ligated into a pmirGLO dual-luciferase miRNA target expression vector (Promega, USA). After that, DPSCs (American Type Culture Collection) were transfected with NC and miR-665 mimics via Lipofectamine 3000 (Invitrogen, USA) for 6 hours in a 24-well plate. After 48-hour transfection, the cells were harvested and lysed, and the luciferase activity was examined using a luciferase assay kit (Promega, USA). Renilla luciferase was acted as internal reference. The assay was repeated 3 times.

Transfection Experiments

Cells were seeded in a 6-well plate one day in advance. When the cell confluence reached 40–60%, transfection was performed. Lipofectamine 3000 reagent (Invitrogen, Carlsbad, CA, USA) was used to transfect the plasmids or oligonucleotides into DPSCs. Afterwards, the mixture was added into each well and cultured in serum-free medium for 6 h. Cells cultured in complete culture medium were further used. The cells were divided into nine groups: miR-665 mimic, miR-665 inhibitor, miRNA mimic control (mimic NC), and miRNA inhibitor control (inhibitor NC), over-expressed PSAT1 (oe-PSAT1), mimic

NC + over-expressed NC (oe-NC), mimic NC + oe-PSAT1, miR-665 mimic + oe-NC, miR-665 mimic + oe-PSAT1. They were all purchased from RIBOBIO (Guangzhou, China).

Fabrication of $Ti_3C_2T_x$ MXene NSs

Ti_3C_2Tx MXene NSs were synthesized according to hydrofluoric acid (HF) etching method. The raw Ti_3AlC_2 powder was etched in the HF solution with a Ti_3AlC_2 concentration of 0.05 g mL^{-1}. The etching reaction was conducted in the Teflon reactor, continuously purging with argon gas at 25 °C for 8 h with continuous stirring. Separated obtained mixture was at a centrifugation speed of 5000 rpm the resultant precipitate was then redispersed into deionized water.

Clean and centrifuge the residual material at 5000 rpm for 5 minutes. Add 25 wt% TMAOH to the precipitate. Fill and seal the conical flask used for the reaction with argon gas. At 30 °C, react at 1000 rpm for 20 hours. Wash and centrifuge the reaction at 5000 rpm three times. For the fourth centrifugation, collect the dark brown supernatant liquid, which is the monolayer MXene dispersion. The dispersion was filtered through a hydrophilic 200 nm polytetrafluoroethylene porous Filter the ethanol through a 0.22 μm aqueous membrane and dry reactants in a vacuum at 50 °C oven for 12 hours.

The morphology of the samples was studied by scanning electron microscopy (SEM, Axia ChemiSEM, Thermo Scientific, USA) and transmission electron microscopy (TEM, Talos F200x, FEI, USA). The crystal structure was analyzed by X-ray diffraction (XRD, D8A25, Bruker, Germany). DPSCs attached to the surface of $Ti_3C_2T_x$ MXene nanosheets were tested by SEM.

Flow Cytometry with FITC-Annexin V/PI Double Staining

After 24 hours of exposure to $Ti_3C_2T_x$ MXene nanoparticles at concentrations of 0, 25, 50, 75, 100, and 150 mg/L, DPSCs were collected. Instead of using EDTA, the cells were incubated for digestion and subsequently centrifuged at 4 °C for 5 minutes. The supernatant above the cell pellet was carefully aspirated. The DPSCs were then rinsed twice with cold PBS, with centrifugation performed after each rinse. Next, an equal volume of Binding Buffer was added, and the mixture was gently pipetted to form a single-cell suspension. Annexin V-FITC and PI staining solutions (Vazyme, China) were added to the suspension, which was then gently mixed. After incubation, another equal volume of Binding Buffer was added and gently mixed. Following the completion of staining, the samples were analyzed using flow cytometry. Specifically, apoptotic cells were identified using a FACS Calibur flow cytometer (BD Biosciences, USA).

ROS Fluorescence Staining of DPSCs

DCFH-DA was used to detected the ROS distribution in the cells. The working solution of DCFH-DA was prepared by mixing DCFH-DA with culture medium at the ratio of 1:1000. DPSCs were seeded in the six-well plate and treated by 25 mg/L $Ti_3C_2T_X$ MXene for 24 h. Then, all cells were cultured for 24 h under oxidative condition (supplemented with 200 μmol L^{-1} H_2O_2). After that, the medium was removed and replaced by the DCFHDA working solution. After 30 min of incubation, all samples were washed three times and observed under a fluorescence microscope (DMi8 S, Leica, Germany).

Animal Studies

Surgical Procedures

All SD rats (7 weeks old, female) were purchased from Laboratory Animal Center of Nantong University. All animal experiments approved by the Animal Ethics Committee of Nantong University (Approval Number: IACUC20220610-1001) and all animal experiments based on the guidelines of the Institutional Animal Care and Use Committee of China. The rats were housed in a barrier environment animal facility at the Animal Experimentation Center of Nantong University. The experimental animals were divided into 3 groups: $Ti_3C_2T_X$ MXene group, oe-NC DPSCs+$Ti_3C_2T_X$ MXene group and oe-PSAT1 DPSCs+ $Ti_3C_2T_X$ MXene group with 8 rats per group. After anesthesia with isoflurane, the hair on the rat's skull was removed, and the skin was disinfected with iodophor followed by alcohol deiodination. The scalp was incised, and the underlying tissues were separated to expose the skull while Separating and protecting the meningeal layer. A full-thickness cranial defect was created on the parietal bone using a surgical drill, with a diameter of 5 mm. Sterile cold saline was continuously dripped during drilling to reduce the temperature. Hemostasis was achieved by gauze compression. 5 mm diameter full-thickness circular defect was created on both sides of the parietal bone, and

The $Ti_3C_2T_X$ MXene with DPSCs complex was secured to the defect area to ensure stable placement using a 10–0 nylon suture to fix the previously separated meningeal layer with the assistance of an operating microscope.

On 8 weeks, the rats were sacrificed. Their major organs (heart, liver, spleen, lung, and kidney) of rats were harvested and fixed at 4 weeks and examined by H&E staining to investigate the in vivo toxicity of $Ti_3C_2T_X$ MXene and DPSCs.

Micro-Computed Tomography (Micro-CT)

All cranial samples were scanned by the Micro-CT instrument (Hiscan XM, Suzhou Hiscan Information Technology Co. Ltd.) with resolution of 10 μm. After scanning, the coronal view and transverse view images were reconstructed by the CT-Volume (Hiscan Analyser (version 3.0)) software.

Histology and Immunohistochemical Staining

All cranial samples were decalcified for 30 days. Afterwards, the decalcified samples were embedded parallel to the sagittal plane of the skull, with the section thickness set to 5 μm, and were stored at 4 °C. Then, the cranial samples sections were subjected to H&E staining and Masson staining to evaluate the effects on bone formation. In addition, immunohistochemical staining for Col I and OPN were performed to evaluate the effects on bone formation. Finally, H&E staining of the heart, liver, spleen, lungs, and kidneys was performed to evaluate the in vivo biocompatibility. The stained sections were photographed under a microscope (BX41, OLYMPUS).

Statistical Analysis

The data were analyzed and expressed as the mean ± standard deviation (SD). Tukey's test and Brown-Forsythe test was used in multiple-comparison test and ANOVA individually. The statistical differences were determined by SPSS 25.0 software. Differences with a $P < 0.05$ were considered statistically significant. Each of the experiments was run in triplicate.

Results

MiR-665 Expression Increased in High Concentration TNF-α (20 ng/mL) Treated DPSCs with Osteogenic Differentiation Repressed

In order to assess the impact of miR-665 on bone formation in the presence of inflammation, DPSCs were grown in a specialized medium that promotes bone formation (osteogenic induction medium, OIM) for 7, 14, and 21 days. Using quantitative real-time PCR, our findings demonstrated a significant increase in the expression level of miR-665 in the presence of a high concentration of TNF-α (20 ng/mL). However, the expression of miR-665 was notably decreased in both the OIM group and the OIM group treated with TNF-α at a lower concentration (10 ng/mL) (Figure 1A). It was found a negative relationship between the expression of miR-665 and osteogenic marker proteins (Figure 1B and C). Further, DPSCs were cultured in OIM with TNF-α (20 ng/mL), and the protein expression level of BMP2, RUNX2, and OPN was tested by Western blot as well as immunofluorescent staining. Transfection miR-665 inhibitor reversed the decrease of DPSCs osteogenic differentiation (Figure 1D–G) which had been proved by Alizarin red staining and ALP activity (Figure 1H–I). MiR-665 mimic or inhibitor would not affect the proliferation of DPSCs (Figure 1J).

PSAT1 Played a Role in the Osteogenic Differentiation of DPSCs That Was Stimulated by TNF-α

To investigate the osteogenic mechanism of PSAT1 under the inflammation micro-environment, DPSCs were cultured in OIM, OIM+TNF-α (10 ng/mL), OIM+TNF-α (20 ng/mL) for 7 days. The level of PSAT1 expression in the OIM+TNF-α (20 ng/mL) group decreased significantly compared to OIM and OIM+TNF-α (10 ng/mL) groups (Figure 2A and B). Immunofluorescence also showed a significant decrease of PSAT1 in the 20 ng/mL group (Figure 2C and D). When PSAT1 over-expressed in DPSCs cultured in OIM+TNF-α (20 ng/mL), the expression of BMP2, RUNX2 and OPN were improved (Figure 2E and F). Alizarin red staining and ALP also proved the inhibition of DPSCs osteogenic differentiation was reversed (Figure 2G and H).

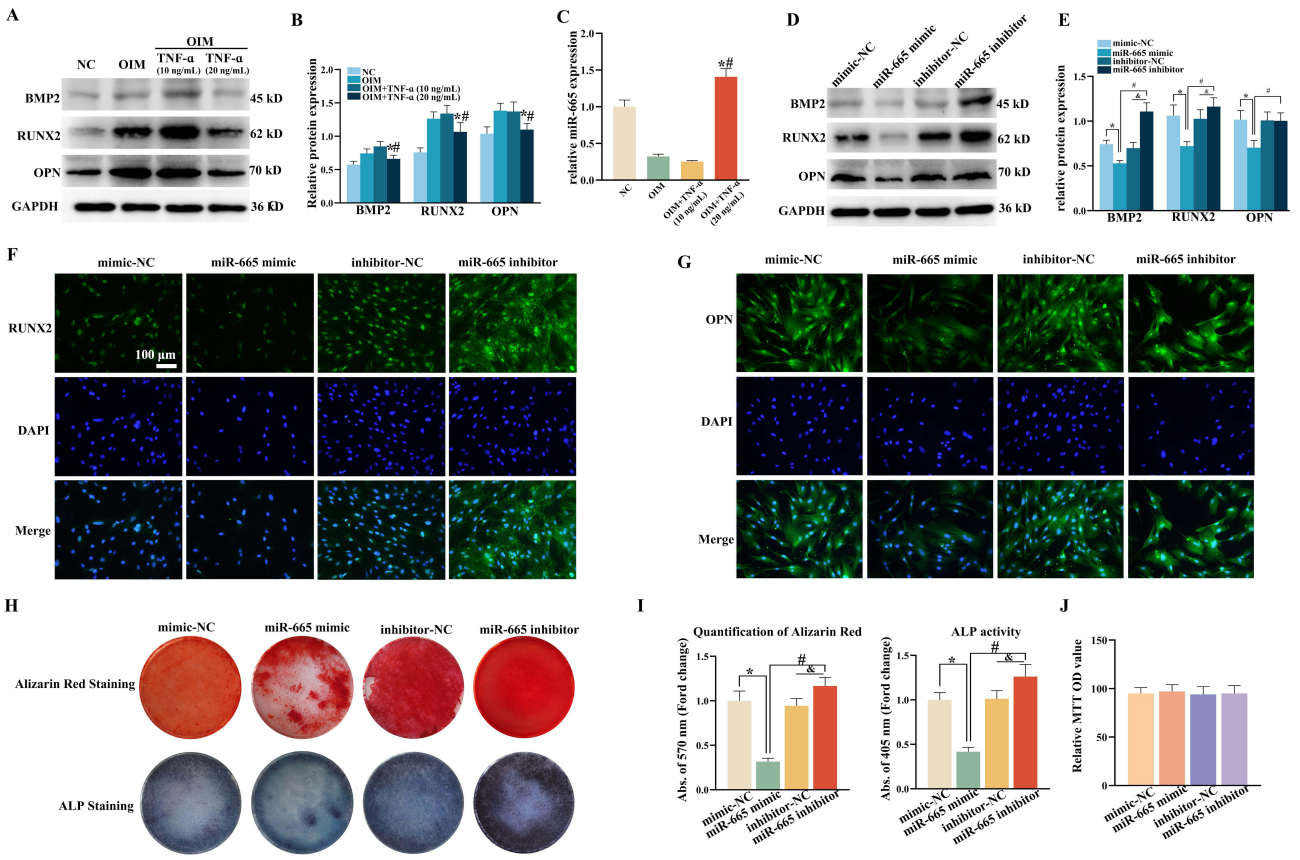

Figure 1 miR-665 inhibited the osteogenic differentiation of DPSCs under TNF-α stimulation. (**A** and **B**) DPSCs were cultured in an osteogenesis induction medium (OIM) for 7 days under different concentrations TNF-α and the expression of BMP2, RUNX2, and OPN was tested by the western bolt (n = 3). * $P < 0.05$ compared with OIM group, # $P < 0.05$ compared with OIM + TNF-α (10 ng/mL) group. (**C**) The expression of miR-665 was tested by qRT-PCR after cultured the same condition as in A, * $P < 0.05$ compared with OIM group, # $P < 0.05$ compared with OIM + TNF-α (10 ng/mL) group. (**D** and **E**) DPSCs were cultured in OIM with TNF-α (20 ng/mL) for 7 days, and different miRNA plasmids were transfected in DPSCs. BMP2, RUNX2, and OPN were detected by Western blot (n = 3). (**F** and **G**) RUNX2 and OPN were detected by immunofluorescent staining (n = 3). * $P < 0.05$ compared with NC-mimic, # $P < 0.05$ compared with miR-665 mimic, & $P <$ compared with inhibitor-NC. (**H** and **I**) DPSCs were cultured in the same condition for 14 days and 21 days. ALP staining and Alizarin red staining of DPSCs was tested (n = 3). * $P < 0.05$ compared with NC-mimic, # $P < 0.05$ compared with miR-665 mimic, & $P < 0.05$ compared with inhibitor-NC. (**J**) MTT assay the proliferation of DPSCs cultured.

PSAT1 May Be a Target Gene of miR-665 in DPSCs Osteogenic Differentiation

The ENCORI method was utilized to forecast the target molecules of miR-665, and it was determined that PSAT1 satisfied the criteria as the target gene (Figure 3A). The group in which miR-665 mimic was co-transfected with luciferase reporter containing the wild-type PSAT1 showed a significant decrease in luciferase activity (Figure 3B). It was found that the protein expression level of PSAT1 was suppressed markedly by miR-665 mimic, while reversed by a miR-665 inhibitor (Figure 3C and D).

GSK-3β/β-Catenin Was Involved in DPSCs Osteogenic Differentiation Regulated by miR-665/PSAT1 Under TNF-α Stimulation

To further confirm the regulation relationship of miR-665/PSAT1 in terms of DPSCs osteogenic differentiation under inflammation micro-environment, the overexpression vector of PSAT1 was structured. Transfection efficiency of the PSAT1 overexpression vector had been proved in Figure 2D. The expression of BMP2, RUNX2, and OPN was significantly up-regulated by overexpression of PSAT1 despite miR-665 mimic compared to miR-665 mimic + oe-NC group, whereas the results in miR-665 mimic group decreased significantly compared to mimic NC group (Figure 4A–D). ALP staining and Alizarin red staining also proved the same results (Figure 4E and F). Further, the expression of p-β-catenin/β-catenin and p-GSK-3β/GSK-3β was also harvested and tested under the same culture condition. The expression of GSK-3β and β-catenin changed not significantly in all

https://doi.org/10.2147/IJN.S521957

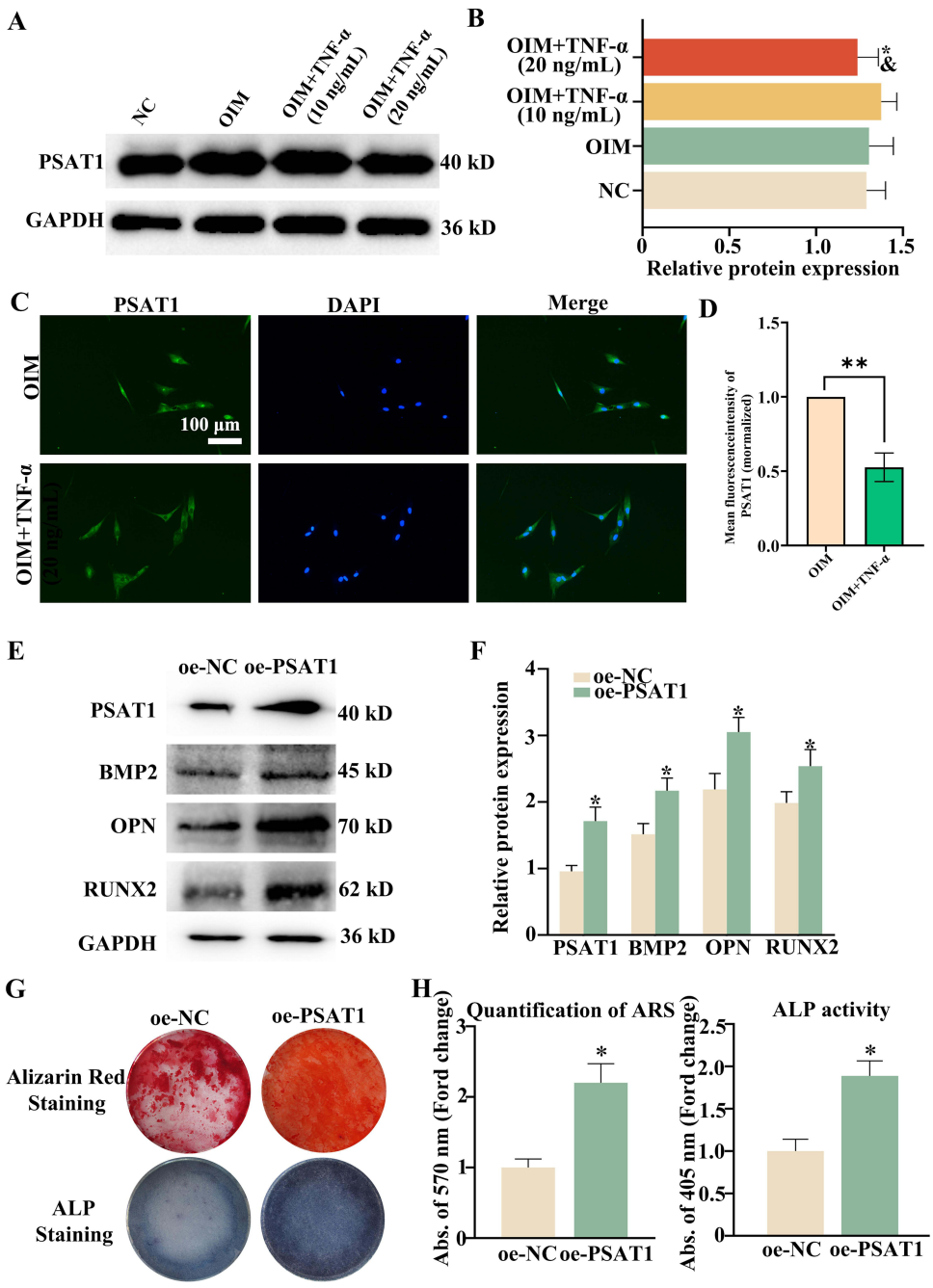

Figure 2 Over-expression PSAT1 promoted the osteogenic differentiation of DPSCs. (**A** and **B**) The expression of PSAT1 was tested by the western bolt in different culture conditions. * $P < 0.05$ compared with OIM group, and $P < 0.05$ compared with OIM + TNF-α (10 ng/mL) group. (**C**) The expression comparison of PSAT1 was tested by immunofluorescence between OIM and OIM + TNF-α (20 ng/mL). (**D**) Corresponding mean fluorescence intensity of PSAT1 in DPSCs. Values were normalized by OIM group. ** $P < 0.01$. (**E** and **F**) PSAT1 overexpression vector was transfected in DPSCs, and the transfection efficiency was tested by Western blot. Meanwhile, BMP2, RUNX2, and OPN were also detected (n = 3). * $P < 0.05$ compared with empty vector. (**G** and **H**) ALP staining and Alizarin red staining of DPSCs was tested (n = 3). * $P < 0.05$ compared with empty vector. All DPSCs were cultured for 7 days in different conditions for Western blot, and 14 days and 21 days for ALP staining and Alizarin red staining.

groups, whereas the expression of p-β-catenin and p-GSK-3β was consistent with BMP2, RUNX2, and OPN (Figure 4G and H). The nuclear expression of β-catenin increases in miR-665 mimic + oe-PSAT1 group (Figure 4I).

Synthesis and Characterization of Ti_3C_2Tx MXene

We used SEM to analyze Ti_3AlC_2 MAX and Ti_3C_2Tx MXene, and the bulk Ti_3AlC_2 MAX showed some bright stripes, but there was no aligned nanowire between the layered structures and no obvious delamination (Figure 5A). However, SEM

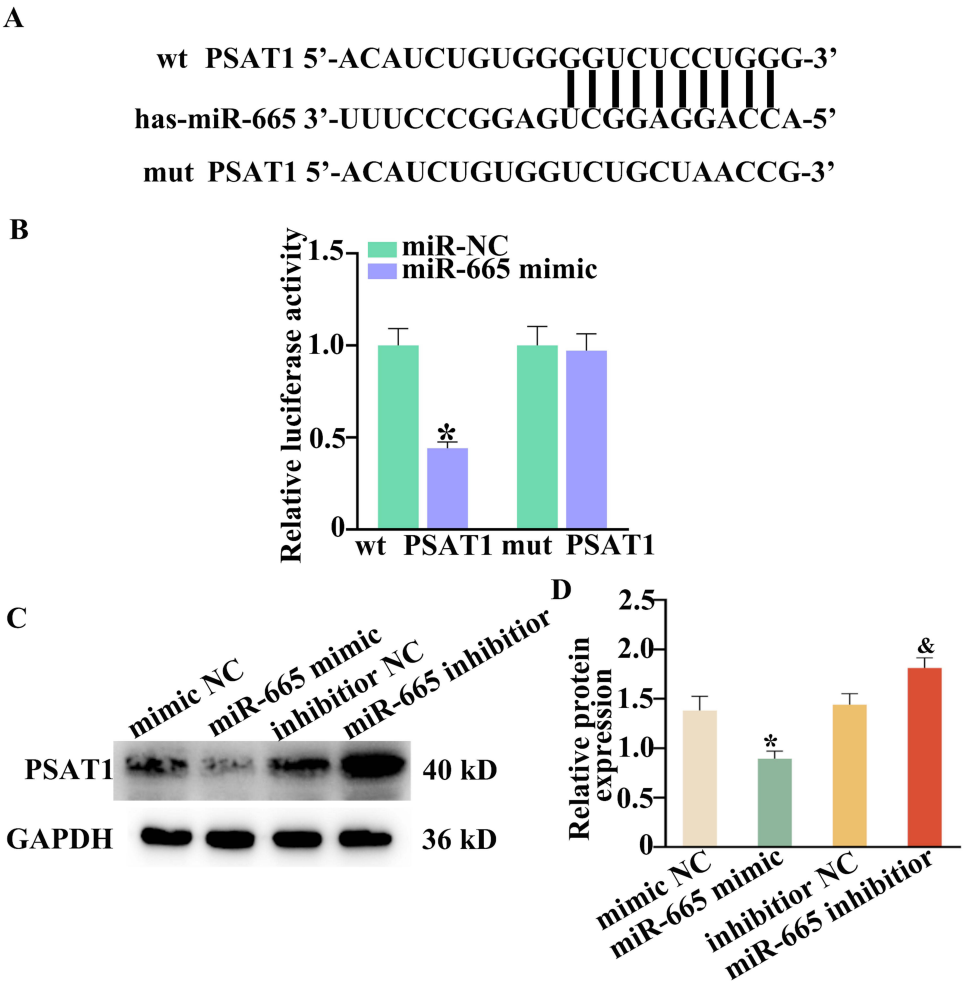

Figure 3 MiR-665 targeted PSAT1 during osteogenic differentiation of DPSCs under inflammatory condition. MiR-665 targeted PSAT1 during osteogenic differentiation of DPSCs under OIM + TNF-α. (**A**) The binding sites of miR-665 targeted PSAT1 predicted by ENCORI (https://starbase.sysu.edu.cn/index.php). (**B**) Dual-luciferase assay of DPSCs cells co-transfected with miR-665 mimic and luciferase reporter containing wild-type 3'-UTR of PSAT1 with or without binding site mutant (n = 3). NC-mimic as a control group. * $P < 0.05$. (**C** and **D**) The expression of PSAT1 in protein level was tested after 7 days (n = 3). DPSCs were cultured in OIM + TNF-α (20 ng/mL), and different construction plasmids were transfected. * $P < 0.05$ compared with mimic NC, & $P < 0.05$ compared with inhibitor NC.

observation of the prepared Ti_3C_2Tx MXene showed peeled particles with delamination Figure 5A). After local magnification of Ti_3C_2Tx MXene, we can observe a clear accordion-like structure of the nanosheet which indicated the gap occupied by Al atoms in the monolayer nanosheet is etched, and the nanosheet shows a gap-like structure. The layered structure of the Ti_3C_2Tx MXene nanosheets was observed by TEM imaging (Figure 5B). In addition, HRTEM images show the original two-dimensional layered structure of Ti_3C_2Tx MXene, and the lattice fringe spacing of 0.22 nm can be clearly observed, and the corresponding SAED diffraction suggests its hexagonal symmetry (Figure 5C).

We performed a crystal phase structure characterization analysis of Ti_3C_2Tx MXene prepared by HF etching. We used XRD to compare Ti_3AlC_2 MAX and Ti_3C_2Tx MXene (Figure 5C). The analysis of Ti_3AlC_2 PDF standard card showed a peak at 10° and 40°, namely 002 and 104. In order to further confirm the crystal structure change of Ti_3C_2Tx MXene, it can be obtained by XRD diffraction that only obvious wave peaks can be seen in the range of 5° ~ 10° in the spectral map. The typical XRD peak (002) of Ti_3AlC_2 showed a strong 2θ upshift, and the Al peak (39°) disappeared during erosion and exfoliation, which proved the removal of the Al atomic layer and the expansion of the surface spacing in Ti_3AlC_2 MAX (Figure 5D).

We used HAADF-STEM and EDS images to observe Ti_3C_2Tx MXene and analyze the distribution of titanium (Ti), carbon (C), oxygen (O) and fluorine (F) elements in Ti_3C_2Tx MXene (Figure 5A), and obtained the composition ratio of each element (Figure 5E). We have supplemented a SEM image showing DPSCs attached to the surface of $Ti_3C_2T_x$ MXene nanosheets. This image clearly demonstrates the adherence of DPSCs to the $Ti_3C_2T_x$ MXene (Figure 5F). A schematic diagram illustrating the synthesis of Ti3C2Tx MXene in Figure 5G.

https://doi.org/10.2147/IJN.S521957

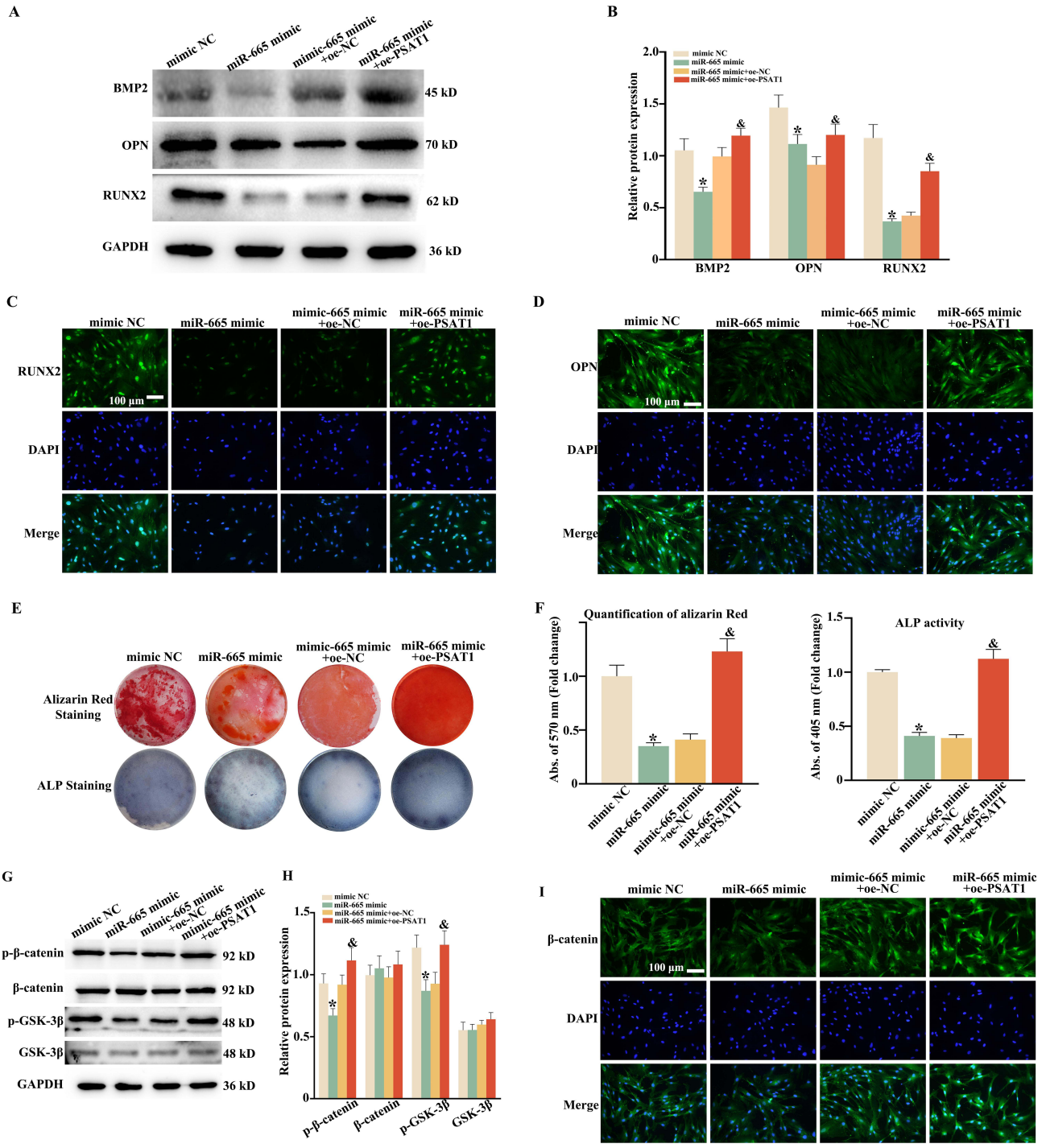

Figure 4 Over-expression PSAT1 reversed the osteogenic differentiation suppression by miR-665. The experiment was divided into four groups: Mimic NC, miR-665 mimic, miR-665 mimic+ov-NC, and miR-665 mimic+oe-PSAT1. (**A**) DPSCs were cultured in OIM + TNF-α (20 ng/mL). Mimic NC, miR-665 mimic, miR-665 mimic+ov-NC, and miR-665 mimic +oe-PSAT1 were transfected in DPSCs respectively. BMP2, OPN and RUNX2 were tested by Western blot (n = 3). GAPDH was used as an internal control. (**B**) Bar groups showing the relative density of BMP2, OPN and RUNX2. (**C** and **D**) RUNX2 and OPN were detected by immunofluorescent staining. (**E** and **F**) ALP staining and Alizarin Red staining of DPSCs was tested. Alizarin Red and ALP staining semiquantitative analysis of DPSCs. (**G** and **H**) The expression of p-β-catenin, β-catenin, p-GSK-3β and GSK-3β has also been tested. (**I**) β-catenin was detected by immunofluorescent staining. * $P < 0.05$ compared with mimic NC, and $P < 0.05$ compared with miR-665 mimic+ov-NC.

Ti_3C_2Tx MXene Promote the Osteogenic Differentiation of Oe-PSAT1 DPSCs in vitro

Flow-cytometry was employed to observe the apoptosis of DPSCs stimulated by different concentrations (0, 25, 50, 75, 100, 150 mg/L) of $Ti_3C_2T_x$ MXene, as shown in Figure 6A. The results indicated that there were minimal differences in the apoptosis arrays among the groups. This suggests that, within the tested concentration range, $Ti_3C_2T_x$ MXene may not

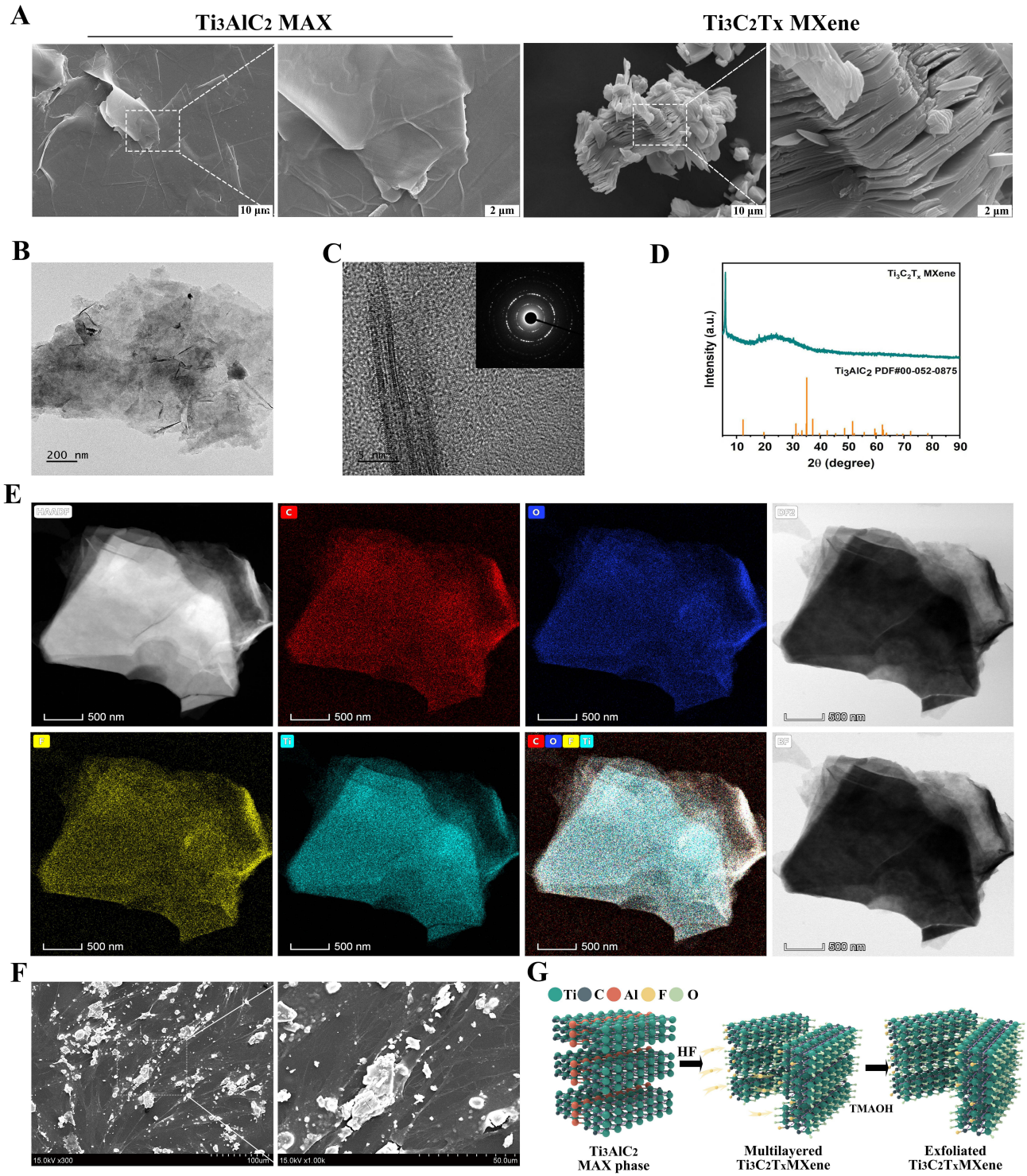

Figure 5 Structural characterization and crystalline phase structure characterization of the assynthesized Ti_3C_2Tx MXene. (**A**) SEM image of the Ti_3AlC_2 MAX and Ti_3C_2Tx MXene and its enlarged area. (**B**) TEM image of the as-exfoliated Ti_3C_2Tx MXene. (**C**) HRTEM image of the as-exfoliated Ti_3C_2Tx MXene; inset: SAED pattern. (**D**) XRD of the as-exfoliated Ti_3C_2Tx MXene. (**E**) HAADF-STEM and EDS images of as-exfoliated Ti_3C_2Tx MXene. (**F**) SEM image of the DPSCs and Ti_3C_2Tx MXene and its enlarged area. (**G**) A schematic diagram illustrating the synthesis of $Ti_3C_2T_x$ MXene.

have a significant impact on the apoptosis of DPSCs. DPSCs morphology did not change significantly after Ti_3C_2Tx MXene treated (Figure 6B). To further explore the in vitro antioxidant properties of Ti_3C_2Tx MXene, DPSCs were treated by Ti_3C_2Tx MXene after H_2O_2 stimulation. Subsequently, the distribution of their intracellular ROS was marked

https://doi.org/10.2147/IJN.S521957

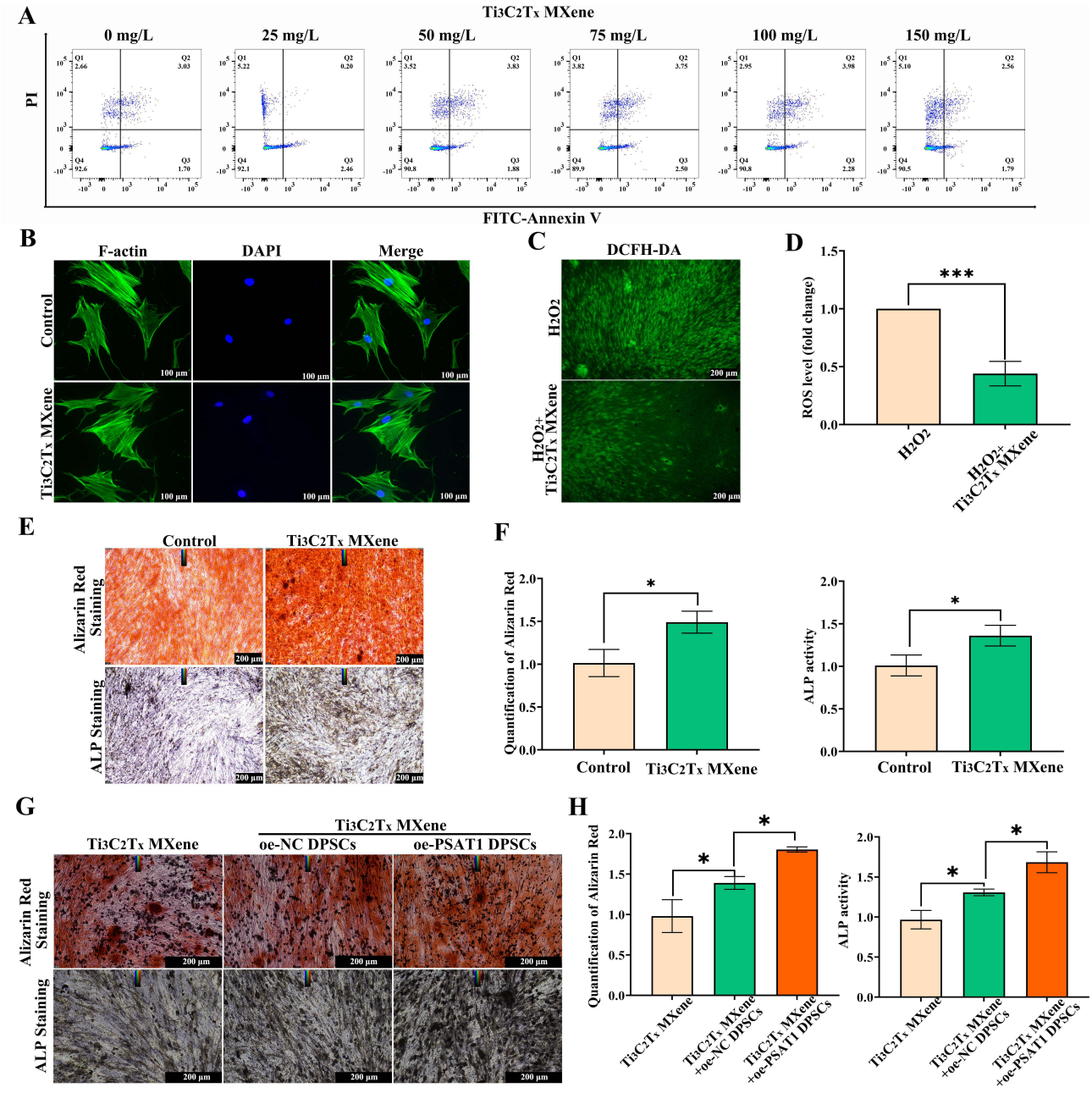

Figure 6 Ti_3C_2Tx MXene promote the osteogenic differentiation of oe-PSAT1 DPSCs in vitro. (**A**) Annexin V^+ and PI^+ cells analyzed by flow cytometry after double staining of DPSCs. (**B**) DPSCs were stained by fluorescein isothiocyanate-conjugated phalloidin. Immunofluorescence showed that the F-actin distribution was normal in DPSCs from Ti_3C_2Tx MXene treated. Scale bars = 100 μm. (**C**) ROS fluorescence staining images in DPSCs cultured with Ti_3C_2Tx MXene under H_2O_2 stimulation. Scale bars = 200 μm. (**D**) Statistical analyze of ROS expression difference multiples detected by immunofluorescence. (**E**) Alizarin Red and ALP staining of DPSCs cultured on 6-well plate, Control and Ti_3C_2Tx MXene for 14 days and 21 days. Scale bars = 200 μm. (**F**) Alizarin Red and ALP staining semiquantitative analysis of DPSCs. (**G**) The experiment was divided into three groups: Ti_3C_2Tx MXene, Ti_3C_2Tx MXene+oe-NC DPSCs and Ti_3C_2Tx MXene+oe-PSAT1 DPSCs. Alizarin Red and ALP staining of DPSCs cultured on 6-well plate for 14 days and 21 days. Scale bars = 200 μm. (**H**) Alizarin Red and ALP staining semiquantitative analysis of DPSCs. Data are expressed as mean ± SD, n = 3. *$p < 0.05$, ***$p < 0.001$.

as green fluorescence by DCFH-DA indicator. As shown in Figure 6C and D, after H_2O_2 stimulation, DPSCs showed obvious green fluorescence. Similarly, after being treated with Ti_3C_2Tx MXene, their intracellular ROS still obviously remained. This finding suggests that Ti_3C_2Tx MXene exhibits antioxidative properties by effectively scavenging excessive ROS within the microenvironment, thereby providing protection to cells against oxidative stress.

The osteogenic differentiation activities of DPSCs were investigated by ARS and ALP staining. As shown in Figure 6E and F, Ti_3C_2Tx MXene could enhance the alkaline phosphatase synthesis and formation of calcium nodules (Figure 6E and F). Ti_3C_2Tx MXene +oe-PSAT1 DPSCs possess more osteogenic differentiation ability compared to Ti_3C_2Tx MXene +oe-NC DPSCs group (Figure 6G and H).

Ti_3C_2Tx MXene Combined Oe-PSAT1 DPSCs Enhanced Bone Regeneration in a Cranial Defects Model of Rats

To evaluate their regenerative effects in vivo, Ti_3C_2Tx MXene +oe-PSAT1 DPSCs were implanted into the cranial defects model of rats. The regeneration effects of cranial bone were assessed by H&E, Masson staining and Micro-CT reconstruction. As shown in Figure 7A–C, after 8 weeks of repair, there were still cavities in the defects of the Ti_3C_2Tx

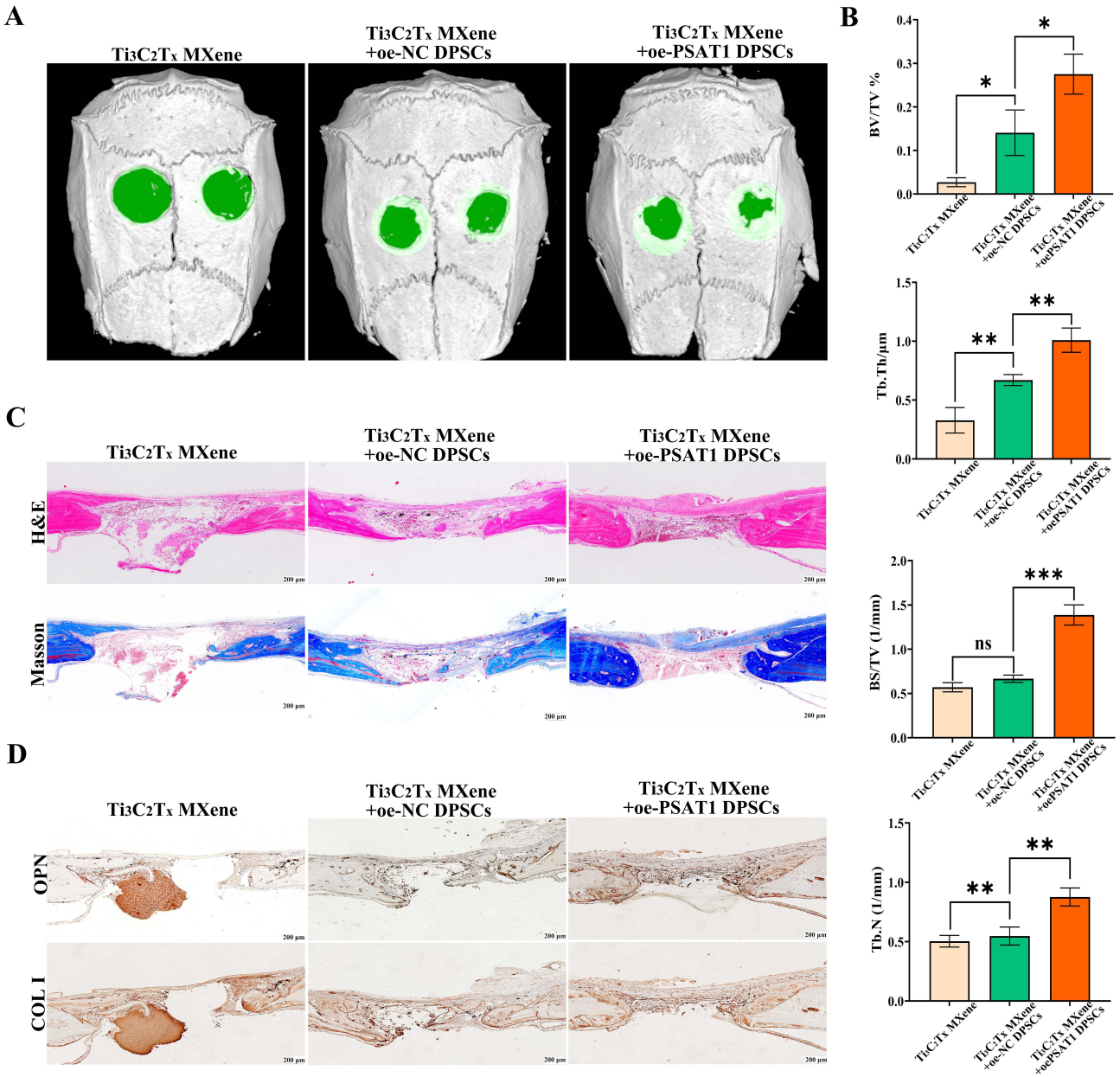

Figure 7 Ti_3C_2Tx MXene combined oe-PSAT1 DPSCs enhanced bone regeneration in a cranial defects model of rats. (**A**) 3D reconstruction of cranial defects at 8 weeks after s Ti_3C_2Tx MXene and oe-PSAT1 DPSCs implantation. (**B**) Quantitative analysis of BV/TV, Tb.Th, BS/TV and Tb.N at 2 months post-surgery based on micro-CT scanning. (**C**) H&E staining and Masson staining of harvested craniums obtained from SD rats after operation. (**D**) IHC evaluation of the bone formation of OPN and COL I at cranial tissue. Scale bars = 200 μm. Data are expressed as mean ± SD, n = 3. ns (not significant), *$p < 0.05$, **$p < 0.01$, ***$p < 0.001$.

https://doi.org/10.2147/IJN.S521957

MXene group. In contrast, in the Ti_3C_2Tx MXene +oe-PSAT1 DPSCs group, new bone had completely covered the defect. Besides, the defects of Ti_3C_2Tx MXene +oe-NC DPSCs groups, only a small amount of new bone grew. BV/TV, Tb.Th, BS/TV and Tb.N were the most highest in Ti_3C_2Tx MXene +oe-PSAT1 DPSCs group.

The images of IHC staining further showed that after 8 weeks, the contents of OPN and COL I protein related to osteogenesis protein related osteoblast maturation in the Ti_3C_2Tx MXene +oe-PSAT1 DPSCs group were higher than those in the other two groups (Figure 7D). The H&E staining results of the main organs (heart, liver, spleen, lung, and kidney) of the Rat showed that Ti_3C_2Tx MXene combined oe-PSAT1 DPSCs did not cause obvious organ damage (Figure 8).

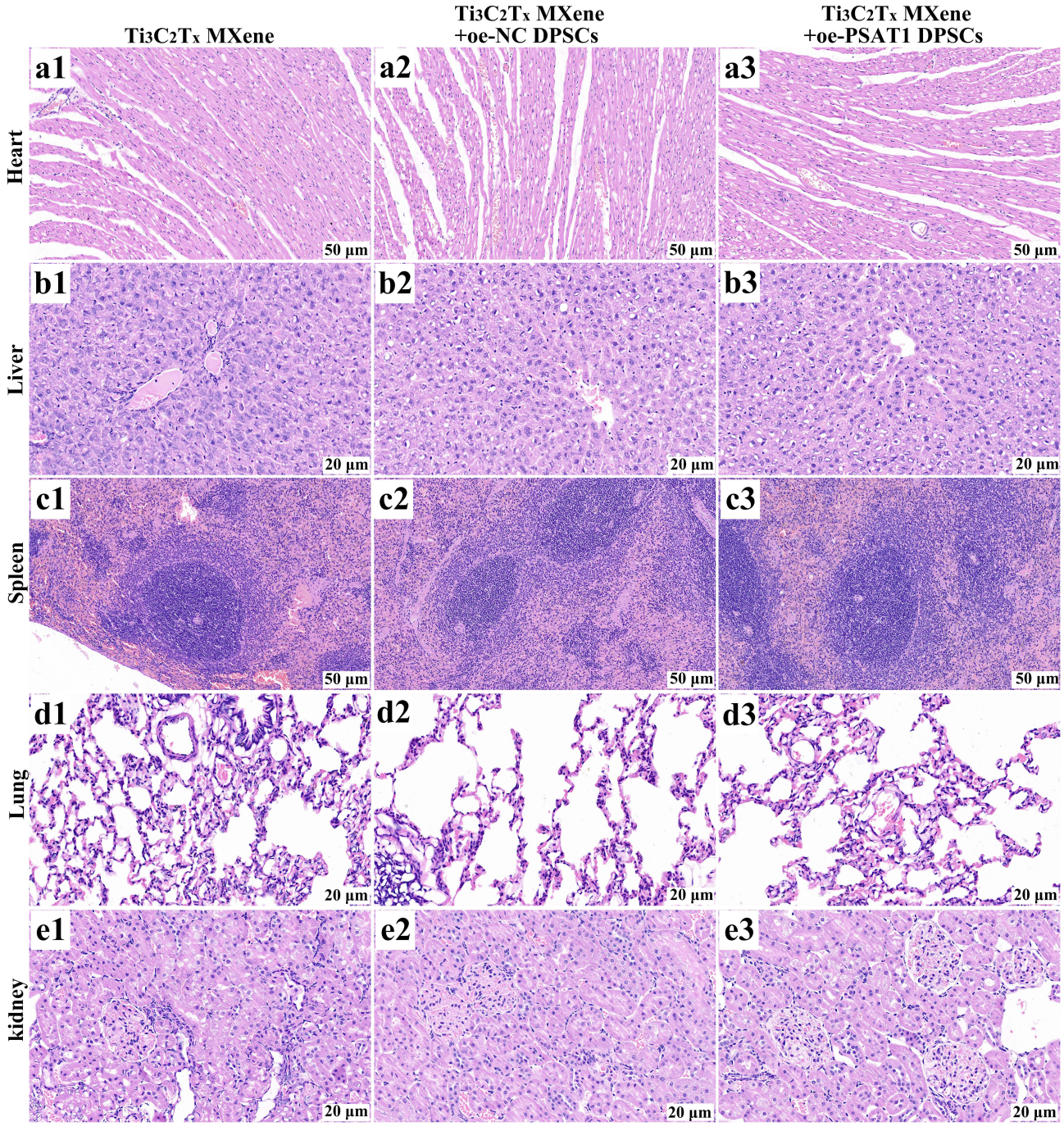

Figure 8 The biosafety evaluation of Ti_3C_2Tx MXene in vivo. (**a1-e3**) Representative images of H&E staining for major organs (heart, liver, spleen, lung and kidney) of rats receiving Ti_3C_2Tx MXene, Ti_3C_2Tx MXene+oe-NC DPSCs and Ti_3C_2Tx MXene+ oe-PSAT1 DPSCs, scale bar = 50 or 20 μm.

Discussion

Stem cell transplantation in the clinic is frequently accompanied by an inflammatory microenvironment, which has an impact on the ability of stem cells to self-renew and differentiate. In our study, the inflammatory microenvironment was simulated by TNF-α, and the osteogenesis capacity of DPSCs was tested. Our research revealed that the stimulation of 20 ng/mL TNF-α hindered the process of osteogenic differentiation in DPSCs. Additionally, the expression of miR-665 was observed to increase (Figure 5). The expression of PSAT1, which is the gene targeted by miR-665, was reduced. Additionally, the GSK-3β/β-catenin pathway was suppressed. However, the over-expression of PSAT1 compensated for the inhibition of miR-665. Two animal experiments also proved the promoting effect of osteogenic differentiation. Particularly, PSAT1 improved alveolar bone regeneration in periodontitis.

MiR-665 exhibited diverse functions in a range of inflammatory disorders. MiR-665 showed significant decrease in osteoarthritis cartilage tissues, and miR-665 resisted the damage of chondrocytes induced by IL-1β.[29] Nevertheless, nucleus pulposus regeneration was inhibited by up-regulating miR-665 expression in intervertebral disc degeneration[28,30] The key role of miR-665 in inflammatory diseases may need to explore in different disease models individually. Especially, in the osteogenic differentiation model of adipose-derived stem cells, the expression of osteogenesis maker proteins reduced after agomiR-665 transfection,[15] and similar results were observed in our research. Also, miR-665 suppressed the proliferation and migration of vascular smooth muscle cells in atherosclerosis,[31] which might promote calcification. The characteristics of miR-665 in osteogenic models may be useful for clinical.

Serine metabolism has been proved to be closely related to bone metabolism. Microtubule Associated Serine/Threonine Kinase Family Member 4 (Mast4) was shown as a transducer in regulating chondro-osteogenic differentiation of mesenchymal stem cells (MSCs) through TGF-β and Wnt signal, and Mast4$^{-/-}$ mice showed excessive cartilage synthesis while osteoporotic.[32] Another study suggests that composite materials made of nanohydroxyapatite and collagen, along with a serine-rich glycol-phosphoprotein, could be advantageous for promoting the differentiation of osteoblasts into more advanced forms during the early stages of bone formation.[33] We note that these assays collectively confirm the temporal progression of osteogenesis: ALP upregulation (early stage) precedes mineralization (late stage), consistent with our observation that miR-665 inhibition or PSAT1 overexpression enhances both markers under inflammatory conditions. PSAT1, a representative gene implicated in the serine biosynthetic pathway (SSP), was also proved to be related to differentiation and mineral absorption. Gingival stem cells were cultured in the inflammatory microenvironment, IL-1β (1 ng/mL), TNF-α (10 ng/mL), and IFN-γ (100 ng/mL, inflammatory-medium), the expression of PSAT1 increased on Day 3 compared to Day 1.[23] Interestingly, the expression of PSAT1 increased under 10 ng/mL TNF-α while decreased at 20 ng/mL in our study. Furthermore, PSAT1 functioned as a protein involved in the serine biosynthetic pathway, which had an impact on the growth, movement, and infiltration of osteosarcoma cells by regulating metabolic reprogramming.[34] Perhaps it might exist a further relationship between serine metabolism and osteogenesis, which would be worth studying further.

MXenes, a class of two-dimensional materials composed of transition metal carbides and nitrides, have garnered significant attention due to their influence on stem cells.[24,25] Research has found that the addition of MXene materials significantly enhances the structural strength of resins. Studies have shown that Ti_3C_2Tx MXene can stimulate periodontal ligament stem cells to promote osteogenesis by activating the Wnt/HIF-1α signaling pathway, which has a favorable effect on the prognosis of periodontitis.[35] In this study, Ti_3C_2Tx MXene was prepared by HF etching of MAX phase, and its unique layered structure was observed through scanning structure characterization and crystal phase structure characterization, with each layer being an extremely thin nanosheet. After ultrasonic treatment of Ti_3C_2Tx MXene, the few-layer nanosheets formed were observed under TEM, showing fewer layers and a corresponding sharp increase in the mass-specific surface area. This characteristic of having a large effective functional area and a small mass is a unique advantage of MXene.[36] Meanwhile, in this study, we confirmed that Ti_3C2Tx MXene has a good promoting effect on the osteogenic differentiation of DPSCs. Meanwhile, we take advantage of its multi-layer physical structure to construct a composite coating loaded with MXene materials, enhancing bone formation and bone defect repair capabilities. We also combine Ti_3C2Tx MXene with DPSCs to enhance the bone regeneration ability of cranial bone defects.

Based on our results showing that $Ti_3C_2T_x$ MXene promotes osteogenic differentiation of DPSCs (Figure 6) and accelerates cranial defect repair (Figure 7) through scavenging ROS and activating the β-catenin pathway, we propose

several promising clinical directions: The biocompatibility (Figure 8) and osteogenic capacity of $Ti_3C_2T_x$ MXene make it a potential candidate for filling critical-sized bone defects, such as those caused by trauma or tumor resection. Its porous structure (observed via SEM in Figure 5A) allows cell infiltration and nutrient exchange, addressing the limitations of traditional grafts like poor integration. $Ti_3C_2T_x$ MXene could be coated onto orthopedic implants (eg, titanium plates or screws) to improve osseointegration. Its ability to enhance calcium-dependent mineralization (Figure 6D and E) may reduce implant loosening, a common complication in orthopedic surgeries. Given the involvement of DPSCs in dental tissue regeneration, MXene-based composites might be applied in periodontal defect repair or alveolar bone augmentation, complementing existing dental materials like calcium phosphate cements by accelerating bone formation. These applications are supported by our in vivo data showing effective bone regeneration and absence of organ toxicity, laying a foundation for future preclinical trials. We appreciate this insightful comment, which has strengthened the clinical relevance of our work.

This study establishes Ti_3C_2Tx MXene and PSAT1-engineered DPSCs as a promising combinatorial strategy for inflammatory bone regeneration, but several directions warrant further exploration: While we demonstrated that MXene scavenges ROS and synergizes with PSAT1 to activate β-catenin, the precise molecular interactions between MXene's surface properties and PSAT1-mediated serine metabolism remain unclear. Future studies could employ proteomics or metabolomics to identify MXene-induced changes in intracellular metabolites that modulate osteogenic signaling. Given the complexity of inflammatory signaling, combining MXene/oe-PSAT1 DPSCs with inhibitors of pro-inflammatory miRNAs or small molecules targeting GSK-3β may further amplify osteogenic outcomes. Such multi-target approaches could overcome residual inflammatory resistance. Scaling MXene synthesis for large-scale production while maintaining batch consistency is essential. Additionally, evaluating the strategy in larger animal models with critical-sized bone defects would provide preclinical data on scaffold integration, vascularization, and functional recovery. These future directions aim to strengthen the mechanistic understanding, optimize the therapeutic strategy, and accelerate the translation of this work to clinical settings for treating inflammation-related bone disorders.

Abbreviations

ALP, Alkaline Phosphatase; BMP2, Bone Morphogenetic Protein 2; BV/TV, Bone Volume/Tissue Volume; COL I, Type I Collagen; DPSCs, Dental Pulp Stem Cells; GSK-3β, Glycogen Synthase Kinase-3β; LPS, Lipopolysaccharide; MSCs, Mesenchymal Stem Cells; NC, Negative Control; OIM, Osteogenic Induction Medium; OPN, Osteopontin; PBS, Phosphate-Buffered Saline; PSAT1, Phosphoserine Aminotransferase 1; RUNX2, Runt-Related Transcription Factor 2; ROS, Reactive Oxygen Species; SEM, Scanning Electron Microscopy; TEM, Transmission Electron Microscopy; TNF-α, Tumor Necrosis Factor-α; Tb.N, Trabecular Number; Tb.Th, Trabecular Thickness; UTR, Untranslated Region; XRD, X-Ray Diffraction.

Consent for Publication

Informed consent was obtained from the participants of this study.

Acknowledgments

The graphical abstract was supported by Figdraw.

Author Contributions

All authors made a significant contribution to the work reported, whether that is in the conception, study design, execution, acquisition of data, analysis and interpretation, or in all these areas; took part in drafting, revising or critically reviewing the article; gave final approval of the version to be published; have agreed on the journal to which the article has been submitted; and agree to be accountable for all aspects of the work.

Funding

This study was supported by the National Natural Science Foundation of China (82202436, Zhiming Cui, Jinlong Zhang); Nantong City sixth Jiang Hai elite second level municipal training project (No. 2022 II-240), Jinlong Zhang); Science and Technology Projects in Jiangsu Province (BE2023742, Zhiming Cui, Chunshuai Wu, Jinlong Zhang). Project

of Jiangsu Administration of Traditional Chinese Medicine (Grant no. MS2022090, Hongxiang Hong). The Basic Science Research Project of Nantong City (JC22022067, Guanhua Xu), the Clinical Basic Research Special Key Project of Nantong University (2022JZ004, Guanhua Xu) Research and Innovation Team Project of Kangda College of Nanjing Medical University "Risk Study of Coronary Heart Disease after Spinal Cord Injury" (KD2022KYCXTD011, Guanhua Xu), the Scientific Research Project of Nantong Municipal Health Commission (QN2024082, Jingwen Xiao).

Disclosure

The authors declared that they have no conflicts of interest to this work.

References

1. Zhao Z, Liu J, Weir MD, et al. Periodontal ligament stem cell-based bioactive constructs for bone tissue engineering. *Front Bioeng Biotechnol*. 2022;10:1071472. doi:10.3389/fbioe.2022.1071472
2. Bagheri L, Valizadeh H, Dindar-Safa K, et al. Fabricating a robust POSS-PCL nanofiber scaffold for nesting of mesenchymal stem cells: potential application in bone tissue regeneration. *J Biol Eng*. 2022;16(1):35. doi:10.1186/s13036-022-00317-5
3. Thant AA, Ruangpornvisuti V, Sangvanich P, et al. Characterization of a bioscaffold containing polysaccharide acemannan and native collagen for pulp tissue regeneration. *Int J Biol Macromol*. 2023;225:286–297. doi:10.1016/j.ijbiomac.2022.11.015
4. Atila D, Keskin D, Lee Y, et al. Injectable methacrylated gelatin/thiolated pectin hydrogels carrying melatonin/tideglusib-loaded core/shell PMMA/silk fibroin electrospun fibers for vital pulp regeneration. *Colloids Surf B Biointerfaces*. 2023;222:113078. doi:10.1016/j.colsurfb.2022.113078
5. Shen H, Jiang W, Yu Y, et al. MicroRNA-146a mediates distraction osteogenesis via bone mesenchymal stem cell inflammatory response. *Acta Histochem*. 2022;124(6):151913. doi:10.1016/j.acthis.2022.151913
6. Kang M, Huang C, Gajendrareddy P, et al. Extracellular vesicles from TNFalpha preconditioned MSCs: effects on immunomodulation and bone regeneration. *Front Immunol*. 2022;13:878194. doi:10.3389/fimmu.2022.878194
7. Zhao L, Liu L, Wu Z, et al. Effects of micropitted/nanotubular titania topographies on bone mesenchymal stem cell osteogenic differentiation. *Biomaterials*. 2012;33(9):2629–2641. doi:10.1016/j.biomaterials.2011.12.024
8. Zhang Y, Lian M, Zhao X, et al. RICK regulates the odontogenic differentiation of dental pulp stem cells through activation of TNF-alpha via the ERK and not through NF-kappaB signaling pathway. *Cell Biol Int*. 2021;45(3):569–579. doi:10.1002/cbin.11498
9. Zhou R, Shen L, Yang C, et al. Periodontitis may restrain the mandibular bone healing via disturbing osteogenic and osteoclastic balance. *Inflammation*. 2018;41(3):972–983. doi:10.1007/s10753-018-0751-5
10. Yi Y. MicroRNA-mediated epigenetic regulation of inflammasomes in inflammatory responses and immunopathologies. *Semin Cell Dev Biol*. 2024;154(Pt C):227–238. doi:10.1016/j.semcdb.2022.11.006
11. Nugent M. MicroRNAs: Exploring new horizons in osteoarthritis. *Osteoarthritis Cartilage*. 2016;24(4):573–580. doi:10.1016/j.joca.2015.10.018
12. Li M, Zhang S, Qiu Y, et al. Upregulation of miR-665 promotes apoptosis and colitis in inflammatory bowel disease by repressing the endoplasmic reticulum stress components XBP1 and ORMDL3. *Cell Death Dis*. 2017;8(3):e2699. doi:10.1038/cddis.2017.76
13. Qi Y, Han Y, Chen C, et al. Inhibition of microRNA-665 alleviates septic acute kidney injury by targeting Bcl-2. *J Healthcare Eng*. 2022;2022:2961187. doi:10.1155/2022/2961187
14. Heair HM, Kemper AG, Roy B, et al. MicroRNA 665 regulates dentinogenesis through MicroRNA-mediated silencing and epigenetic mechanisms. *Mol Cell Biol*. 2015;35(18):3116–3130. doi:10.1128/MCB.00093-15
15. Wu R, Ruan J, Sun Y, et al. Retraction note: long non-coding RNA HIF1A-AS2 facilitates adipose-derived stem cells (ASCs) osteogenic differentiation through miR-665/IL6 axis via PI3K/Akt signaling pathway. *Stem Cell Res Ther*. 2023;14(1):124. doi:10.1186/s13287-023-03355-y
16. Park S, Seo E, Bae D, et al. Phosphoserine phosphatase promotes lung cancer progression through the dephosphorylation of IRS-1 and a noncanonical L-serine-independent pathway. *Mol Cells*. 2019;42(8):604–616. doi:10.14348/molcells.2019.0160
17. Zhang Y, Li J, Dong X, et al. PSAT1 regulated oxidation-reduction balance affects the growth and prognosis of epithelial ovarian cancer. *Onco Targets Ther*. 2020;13:5443–5453. doi:10.2147/OTT.S250066
18. Yang Y, Wu J, Cai J, et al. PSAT1 regulates cyclin D1 degradation and sustains proliferation of non-small cell lung cancer cells. *Int J Cancer*. 2015;136(4):E39–E50. doi:10.1002/ijc.29150
19. Fang Y, Liang X, Xu J, et al. MiR-424 targets AKT3 and PSAT1 and has a tumor-suppressive role in human colorectal cancer. *Cancer Manage Res*. 2018;10:6537–6547. doi:10.2147/CMAR.S185789
20. Tang X, Luo L, Li Y, et al. Therapeutic potential of targeting HSPA5 through dual regulation of two candidate prognostic biomarkers ANXA1 and PSAT1 in osteosarcoma. *Aging*. 2020;13(1):1212–1235. doi:10.18632/aging.202258
21. Yang RL, Huang HM, Han CS, et al. Serine metabolism controls dental pulp stem cell aging by regulating the DNA methylation of p16. *J Dental Res*. 2021;100(1):90–97. doi:10.1177/0022034520958374
22. Hwang I, Kwak S, Lee S, et al. Psat1-dependent fluctuations in alpha-ketoglutarate affect the timing of ESC differentiation. *Cell Metab*. 2016;24(3):494–501. doi:10.1016/j.cmet.2016.06.014
23. Km Fawzy El-Sayed, Bittner A, Schlicht K, et al. Ascorbic acid/retinol and/or inflammatory stimuli's effect on proliferation/differentiation properties and transcriptomics of gingival stem/progenitor cells. *Cells*. 2021;10(12). doi:10.3390/cells10123310
24. Xuan J, Wang Z, Chen Y, et al. Organic-base-driven intercalation and delamination for the production of functionalized titanium carbide nanosheets with superior photothermal therapeutic performance. *Angew Chem Int Ed Engl*. 2016;55(47):14569–14574. doi:10.1002/anie.201606643
25. Huang K, Li Z, Lin J, et al. Two-dimensional transition metal carbides and nitrides (MXenes) for biomedical applications. *Chem Soc Rev*. 2018;47(14):5109–5124. doi:10.1039/c7cs00838d
26. Cui D, Kong N, Ding L, et al. Ultrathin 2D titanium carbide MXene (Ti3C2Tx) nanoflakes activate WNT/HIF-1α-mediated metabolism reprogramming for periodontal regeneration. *Adv Healthcare Mater*. 2021;10(22):e2101215. doi:10.1002/adhm.202101215

27. Wei C, Chu M, Zheng K, et al. MiR-153-3p inhibited osteogenic differentiation of human DPSCs through CBFbeta signaling. *In Vitro Cell Dev Biol Anim*. 2022;58(4):316–324. doi:10.1007/s11626-022-00665-y
28. Feng X, Xing J, Feng G, et al. Age-dependent impaired neurogenic differentiation capacity of dental stem cell is associated with Wnt/beta-catenin signaling. *Cell Mol Neurobiol*. 2013;33(8):1023–1031. doi:10.1007/s10571-013-9965-0
29. Pan F, Li Z, Luo Y, et al. WITHDRAWN: circ_0136474 contributes to the IL-1beta-induced chondrocyte injury by binding to miR-665 to induce the FGFR1 upregulation. *Transplant Immunol*. 2022:101615. doi:10.1016/j.trim.2022.101615.
30. Yu X, Liu Q, Lu R, et al. Bone marrow mesenchymal stem cell-derived extracellular vesicles carrying Circ_0050205 attenuate intervertebral disc degeneration. *Oxid Med Cell Longev*. 2022;2022:8983667. doi:10.1155/2022/8983667
31. Wang Y, Pei W, Lu P. Circ_ARHGAP32 acts as miR-665 sponge to upregulate FGF2 to promote ox-LDL induced vascular smooth muscle cells proliferation and migration. *Clin Hemorheol Microcirc*. 2022;82(2):169–182. doi:10.3233/CH-221469
32. Kim P, Park J, Lee D, et al. Mast4 determines the cell fate of MSCs for bone and cartilage development. *Nat Commun*. 2022;13(1):3960. doi:10.1038/s41467-022-31697-3
33. Salgado CL, Teixeira BIB, Monteiro FJM. Biomimetic composite scaffold with phosphoserine signaling for bone tissue engineering application. *Front Bioeng Biotechnol*. 2019;7:206. doi:10.3389/fbioe.2019.00206
34. Zhang Y, Gong R, Liu Y, et al. Ailanthone inhibits proliferation, migration and invasion of osteosarcoma cells by downregulating the serine biosynthetic pathway. *Front Oncol*. 2022;12:842406. doi:10.3389/fonc.2022.842406
35. Li R, Zhang L, Shi L, et al. MXene Ti 3 C 2: an effective 2D light-to-heat conversion material. *ACS Nano*. 2017;11(4):3752–3759. doi:10.1021/acsnano.6b08415
36. Naguib M, Mochalin VN, Barsoum MW, et al. 25Th anniversary article: mXenes: a new family of two-dimensional materials. *Adv Mater*. 2014;26(7):992–1005. doi:10.1002/adma.201304138